

1 2020 forest age map for China with 30 m resolution

2 Kai Cheng¹, Yuling Chen¹, Tianyu Xiang², Haitao Yang¹, Weiyan Liu³, Yu Ren^{1,4}, Hongcan Guan⁵,
3 Tianyu Hu⁶, Qin Ma⁷, Qinghua Guo^{1,4*}

4 ¹Institute of Remote Sensing and Geographic Information System, School of Earth and Space Sciences, Peking University,
5 Beijing 100871, China

6 ²College of Earth Sciences, Chengdu University of Technology, Chengdu 610059, China

7 ³State Forestry and Grassland Administration Key Laboratory of Forest Resources & Environmental Management, Beijing
8 Forestry University, Beijing 100083, China

9 ⁴Institute of Ecology, College of Urban and Environmental Sciences, Peking University, Beijing 100871, China

10 ⁵School of Tropical Agriculture and Forestry, Hainan University, Haikou 570100, China

11 ⁶State Key Laboratory of Vegetation and Environmental Change, Institute of Botany, Chinese Academy of Sciences, Beijing
12 100093, China

13 ⁷School of Geography, Nanjing Normal University, Nanjing 210023, China

14

15 *Correspondence to:* Qinghua Guo (guo.qinghua@pku.edu.cn)

16 **Abstract.** A spatially explicit, high-resolution forest age map is critical for quantifying forest carbon stock and carbon
17 sequestration potential. Previous endeavours to estimate forest age in China at national scale mainly concentrated on a sparse
18 resolution or incomplete forest ecosystems because of complex species composition, vast forest areas, insufficient field
19 measurements, and the lack of effective methods. To overcome these limitations, we construct a framework for estimating
20 China's forest age by combining remote-sensing time series analysis with **machine learning algorithms (MLAs)** based on
21 massive field measurements and remote-sensing dataset. Specifically, the LandTrendr time series analysis is first applied to
22 detect forest disturbances from 1985 to 2020, with the time since the last disturbance serving as a proxy for forest age. Next,
23 for pixels where no disturbance, machine learning algorithms are used to estimate forest age from independent variables,
24 including forest height, climate, terrain, soil, and forest-age field measurements. Finally, **MLAs** are established for each
25 vegetation division and used to estimate forest ages. Combining these two methods produces a spatially explicit 30 m resolution
26 forest-age map for China in the year of 2020. Validation against independent field plots produces a R^2 from 0.51 to 0.63.
27 Nationally, the average forest age is 56.1 years (standard deviation = 32.7 years), where the Qinghai-Tibet Plateau alpine
28 vegetation zone has the oldest forest with an average of 138.0 years, whereas the forest in the warm temperate deciduous-
29 broadleaf forest vegetation zone averages only 28.5 years. This 30-m-resolution forest-age map provides vital information for
30 accurately understanding the ecological benefits of China's forests and to sustainably manage China's forest resources **and is**
31 **available at <http://dx.doi.org/10.5281/zenodo.8354262> (Cheng et al., 2023b).**

32 1 Introduction

33 Forest age provides critical information about forest ecosystem succession and condition, making it essential for understanding
34 the ecological benefits of forests (Lin et al., 2023). China's forests have been significantly disrupted in the past few decades
35 due to natural disasters and human activities (Niu et al., 2023), resulting in substantial changes to the forest-age structure. This
36 situation makes it significantly challenging to accurately understand forest ecosystem carbon storage (Pan et al., 2011; Tong
37 et al., 2020). Because of complex species composition, vast forest areas, insufficient field measurements, and the lack of
38 effective methods, existing estimates of the China's forest age on the national scale have concentrated on sparse resolution
39 (Zhang et al., 2017) or incomplete forest ecosystem (Xiao et al., 2023). This brought considerable uncertainties in assessing
40 the carbon sources and sinks in China's forest ecosystem (Piao et al., 2022; Wang et al., 2022). Therefore, there is an urgent
41 need to map time-efficient forest age with high spatial resolution across China.

42 Currently, China's forest age is acquired mainly through the national forest inventory, which is highly accurate (Xiao et al.,
43 2023) but requires extensive labour and material resources and is time-consuming and costly (Liu et al., 2022). Additionally,
44 most of China's forests are in steep mountainous areas that are difficult to access (Cheng et al., 2023a), which limits the survey
45 range and uneven distribution of field samples, making it difficult to estimate the age of China's forests on a national scale.
46 Thus, using the traditional method of forest inventory is difficult to capture the complete age distribution and spatial
47 characteristics of China's forests in a timely and accurate manner.

48 Remote sensing technology has been proved effective in estimating forest cover (Su et al., 2020; Tubiello et al., 2023) and
49 forest structure (Yu et al., 2020a; Maltman et al., 2023a) at multiple scales. The opening and sharing of Landsat time series
50 and the development of Google Earth Engine (GEE) cloud-processing platform has facilitated the application of remote sensing
51 to estimate forest age. **Several studies have been conducted to map China's forest age.** Xiao et al. (2023) mapped the age of
52 China's young forests at 30 m resolution by using continuous change detection and classification (CCDC) method. Yu et al.
53 (2020a) produced a 1-km resolution map of the age for planted forests in China by using the age-height equations. Zhang et
54 al. (2017) proposed a top-down method to generate a 1km stand age map using climate and forest height data. Zhang et al.
55 (2014) mapped a national forest age map with 1 km resolution by using remote-sensing forest height and forest type data.

56 **However, the existing China's forest age maps are typically undertaken at coarser spatial resolutions (e.g., 1 km), while finer**
57 **resolutions (e.g., 30 m) are generated only for young forests.** There is still lacking forest age spatial dataset with high resolution
58 covering all of China's forests region.

59 **Two approaches have generally been used to map forest age.** The first is statistical parametric regression approaches, which
60 estimates forest age through establishing a coherent relationship between remote sensing features and field-collected empirical
61 samples to deduce forest age (Maltamo et al., 2020; Schumacher et al., 2020a). Growth models are one of the most popular
62 parametric models of forest age estimation (Zhang et al., 2014; Zhang et al., 2017; Yu et al., 2020b). However, this type of
63 model is based on tree species, which makes it hard to derive forest age when lacking species information, especially over
64 large scales. The second methodological category is nonparametric machine learning algorithms (MLAs), which are more

65 flexible and can handle complex problems (Alerskans et al., 2022). Currently, the application of MLAs to estimate national
66 forest age has not been widely explored. Some previous studies used a single MLA, such as Random Forest (RF) (Besnard et
67 al., 2021b), to estimate the age of the forest. **However, the wide distribution of forests, complex forest types, and diverse terrain
68 and climate conditions in China make it difficult to apply a single model to determine the national age of forests.** Therefore, it
69 is necessary to explore the applicability of MLAs in the estimation of forest age in different regions of China.

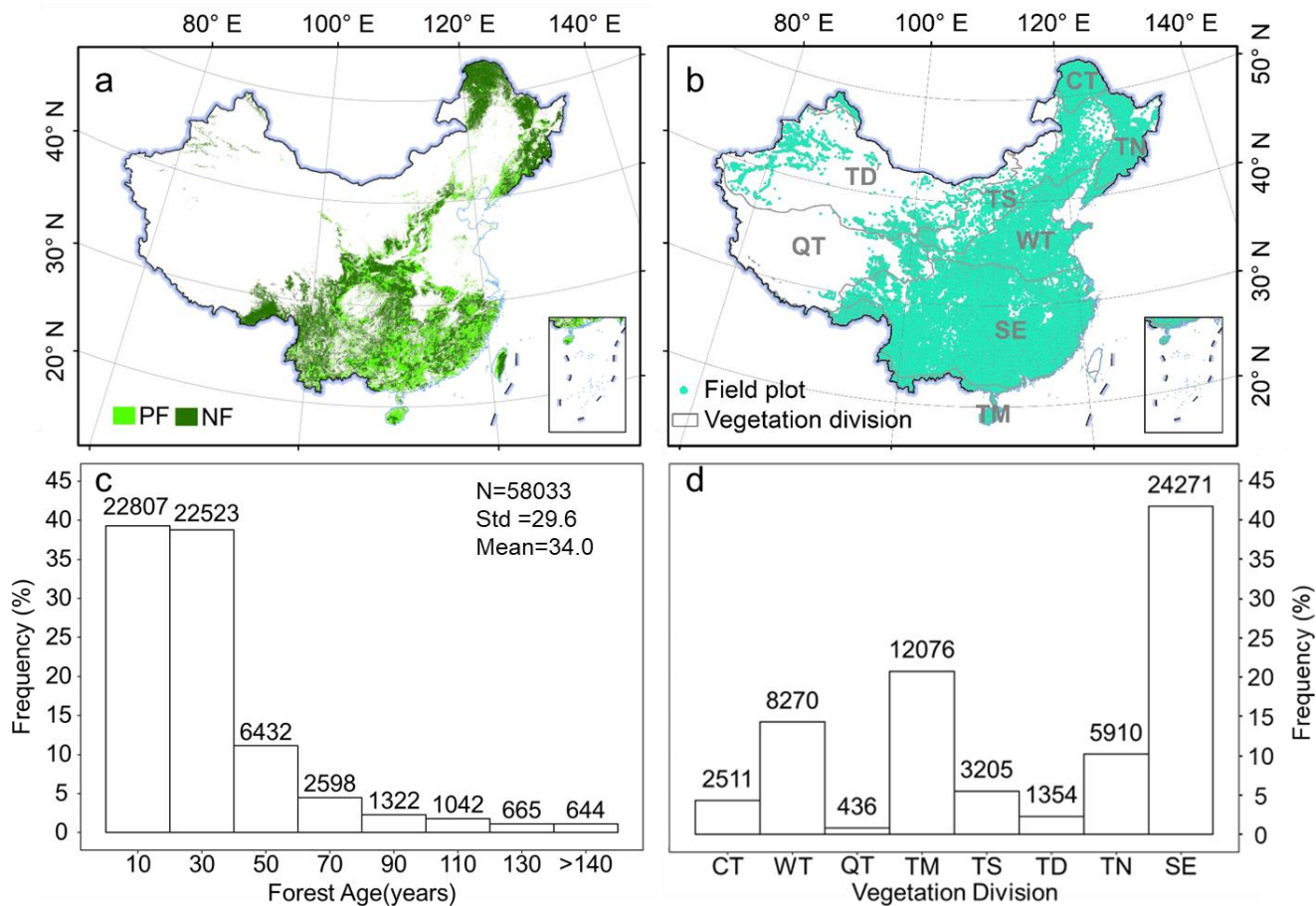
70 The objective of the present study is to generate the first China's forest age dataset at 30 m resolution using multi-source
71 datasets based on remote sensing time series analysis and MLAs. Specifically, first, we apply the LandTrendr change detection
72 algorithm to monitor forests disturbed between 1985 and 2020 to estimate their ages. Subsequently, utilizing mainstream
73 machine learning algorithms, we engage in a zone-based exploration to determine the optimal models for forest age estimation
74 in undisturbed areas to estimate forest age. Finally, the resulting forest age map is validated by using forest field measurements
75 and existing remote sensing products. The generated 30-m-resolution forest age map provides critical information to quantify
76 forest carbon storage and to sustainably manage China's forests.

77 **2 Materials and methods**

78 **2.1 Dataset and pre-processing**

79 **2.1.1 Forest inventory data**

80 The data from China's seventh national forest inventory survey from 2004 to 2008 (<http://www.forestry.gov.cn/>) were
81 collected to develop models to estimate forest age. The inventory involves systematically and accurately monitoring the
82 national forest resources based on **667m² sample** plots covering the whole country (Ren et al., 2011). The main information
83 collected from the sample plots are tree species, stand age, average tree height, and geographic location. The stand age is
84 determined based on the planting time or is estimated using tree diameter at breast height (Zhang et al., 2017). We totally
85 collected 58,033 field plots ranging in age from 1 to 480 years (Figures 1b and 1c). The mean age of the samples is 34.0 years,
86 with a standard deviation of 29.6 years. The sample plots were distributed across eight vegetation divisions (Figure 1b), each
87 containing at least 436 sample plots for building MLA models to estimate forest age (Figure 1d).



88

89 Figure 1. Forest mask and field sample distribution. (a) Planted forest and natural forest mask generated by Cheng et al. (2023a).

90 (b) Distribution of field samples over eight vegetation divisions. (c) Frequency distribution of field sample ages. (d) Frequency

91 distribution of field samples for eight vegetation divisions. PF: planted forest, NF: natural forest, CT: Cold Temperate

92 needleleaf forest, WT: Warm Temperate deciduous-broadleaf forest, QT: Qinghai-Tibet Plateau alpine vegetation, TM:

93 Tropical Monsoon forest-rainforest, TS: Temperate Steppe, TD: Temperate Desert, TN: Temperate Needleleaf-broadleaf

94 mixed forest, SE: Subtropical Evergreen broadleaf forest. N: the number of plots, Std: standard deviation, Mean: mean age.

95 2.1.2 Landsat time-series data

96 From the GEE platform, we collected Landsat TM, ETM+, OLI Tier 1 surface reflectance images dating from 1985 to 2020

97 to estimate forest age for disturbed forest regions. All data were atmospherically corrected and processed by the Land Surface

98 Reflectance Code and the Landsat Ecosystem Disturbance Adaptive Processing System algorithms. We removed the clouds

99 or cloud shadows using the C function of the mask algorithm (Du et al., 2023), then we created composited images using a

100 median compositing method for forest regions. Finally, we calculated the normalized burn ratio (NBR) to detect forest

101 disturbance. NBR has been proved effective in numerous studies detecting forest disturbance (Du et al., 2023; Tian et al.,
102 2023). It is calculated as follows by using the near-infrared (NIR) and short-wave infrared (SWIR) bands:

$$NBR = \frac{NIR - SWIR}{NIR + SWIR} \quad (\text{Eq. 1})$$

103 **2.1.3 Forest mask**

104 This study uses the 2020 dataset of planted and natural forests at 30 m resolution in China (Figure 1a) as a mask for forest age
105 mapping. This dataset is produced by integrating multisource remote-sensing data and a large number of crowdsourced samples,
106 with an overall accuracy of over 80% (Cheng et al., 2023a). In this study, we employ this dataset as a forest mask and utilize
107 a combination of time series change detection algorithms and MLAs to trace the age of these planted and natural forests.

108 **2.1.4 Forest height data**

109 The canopy height data for China was downloaded from the website (<https://3decology.org/>), which was generated based on
110 deep learning by integrating Global Ecosystem Dynamics Investigation and Ice, Cloud and land Elevation Satellite -2 data.
111 This dataset has a spatial resolution of 30 m and corresponds to 2019. The accuracy of this national forest canopy height data
112 was assessed by comparing three independent validation datasets, indicating high accuracy for the canopy height product by
113 neural network guided interpolation ($R^2 \geq 0.55$, $RMSE \leq 5.5$ m) (Liu et al., 2022). Notably, the forest extent used in this dataset
114 is consistent with the forest extent mentioned earlier for planted and natural forests, ensuring spatial consistency when
115 estimating forest age.

116 **2.1.5 Climate data**

117 Climate data were acquired from **WorldClim** 2.1 (<https://worldclim.org/>), which offers 19 bioclimatic variables, including
118 temperature and precipitation, with 30 arc-second resolutions. The 19 bioclimatic variables include annual trends, seasonality,
119 and extreme environmental factors in temperature and precipitation. We resampled the 19 GeoTiff (.tif) files to 30 m resolution
120 using a nearest-resampling method for spatial resolution consistency. To reduce the dimension of bioclimatic variables, we
121 applied a principal component analysis to map the 19 bioclimatic variables into a new principal component (PC) space. We
122 use the first three components PC1, PC2, PC3 to represent the climate factors. According to the results of the analysis, PC1
123 gives annual trends in temperature and precipitation, PC2 gives seasonal variations in temperature and precipitation, and PC3
124 gives precipitation and temperature extremes (Supplementary Table 1).

125 **2.1.6 Soil data**

126 Soil data were extracted from the harmonized world soil database, V1.2, developed jointly by the Food and Agriculture
127 Organization of the United Nations, the International Institute for Applied Systems, the ISRIC-World Soil Information, the
128 Institute of Soil Science, Chinese Academy of Sciences, and the Joint Research Centre of the European Commission with a

129 resolution of 30 arc-seconds. As per previous studies, soil type and texture were selected from the soil dataset in this study to
 130 construct the model to estimate forest age (Besnard et al., 2021a). We also resampled the soil data to 30 m using a nearest-
 131 resampling method.

132 2.1.7 Topographic data

133 The Shuttle Radar Topography Mission (SRTM) V3 provides global digital elevation data at 30 m resolution and was used in
 134 this study to extract topographic variables (Su et al., 2020). Three topographic features, elevation, slope, and aspect, were
 135 calculated to estimate forest ages.

136 **Table 1.** Descriptions of variables used to estimate the forest age of China.

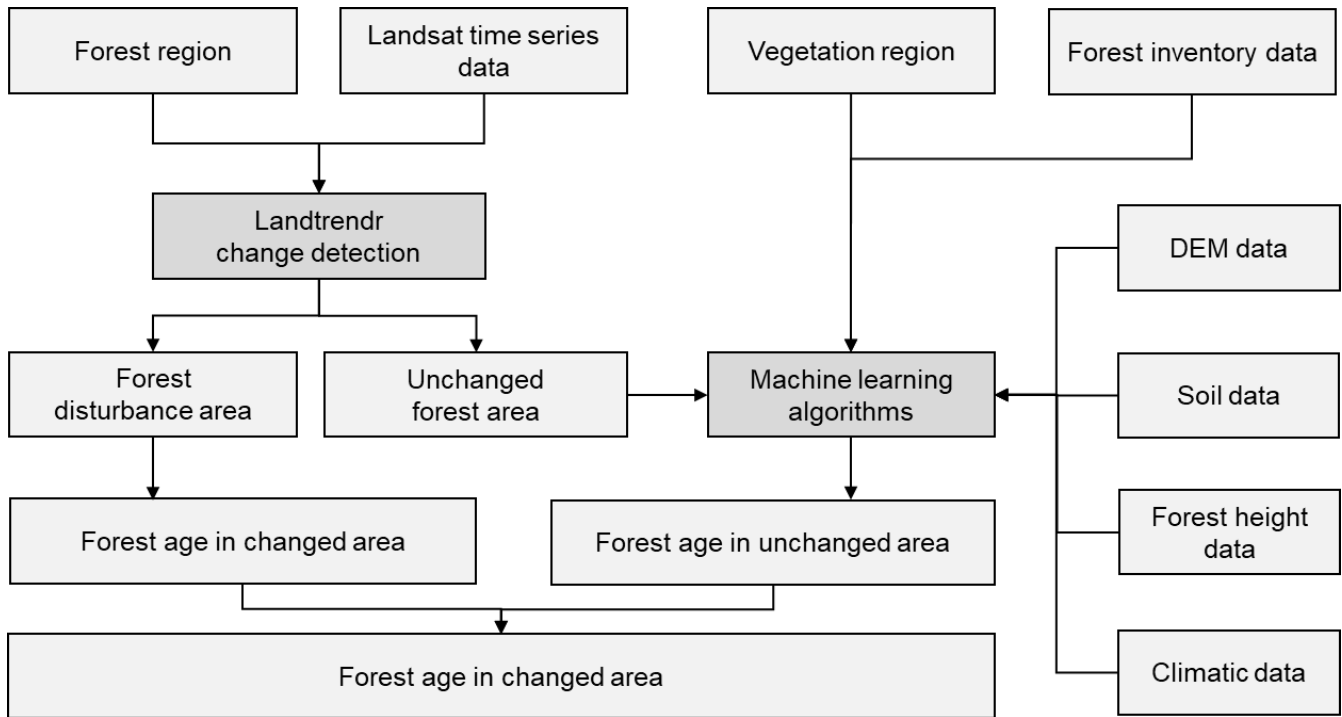
Data type	Data source	Resolution	Time	Variables
Remote sensing images	Landsat TM/ETM+/OLI	30m	1985– 2020	NBR
Forest mask	Planted and natural forest map (Cheng et al., 2023a)	30m	2020	Planted and natural forest
Forest canopy height data	NNGI-Forest Canopy Height	30m	2019	Forest height
Climate data	WorldClim version 2.1 (Fick and Hijmans 2017)	1 km	1970– 2000	PC1, PC2, PC3
Soil data	Harmonized World Soil Database V1.2(https://www.fao.org/soils-portal/data-hub/soil-maps-and-databases/harmonized-world-soil-database-v12/en/)	30 arc-second	1971– 1981	Soil type, soil texture
Topographic data	SRTM DEM	30 m	2000	Elevation, slope, and aspect

137

138 2.2 Forest age estimation

139 To generate the forest age map for China and explore the performance of MLAs to retrieve forest age, we applied two
 140 approaches to estimate forest age in China: the LandTrendr detection approach and the MLA-based approach. First, the
 141 LandTrendr was applied to detect stand-replacing disturbances based on the Landsat time series images. Second, the MLA-
 142 based method estimated ages for undisturbed forest regions within Landsat time series data. Here, we assumed that undisturbed

143 forests over the Landsat record (before 1985) have the similar structural and spectral features to natural forests. Figure 2 shows
 144 a detailed flowchart describing the framework for forest age estimation proposed in this study.



145
 146 **Figure 2.** Framework of China's forest age estimation.

147

148 2.2.1 LandTrendr detection approach

149 LandTrendr was designed to detect and analyse changes in surface features, particularly disturbances and recovery processes,
 150 and is commonly applied to multispectral remote sensing imagery from the Landsat satellite series to capture long-term forest
 151 disturbances (Du et al., 2022). Using LandTrendr to detect forest age involves the following steps:

152 (1) Time series data transformation. LandTrendr transforms multiple temporal remote-sensing image datasets into a series of
 153 indices, such as the NBR.

154 (2) Breakpoint detection. Using the generated time series indices, LandTrendr retraces from the state in 2020 in search of
 155 breakpoints in the time series. These breakpoints signify transition points in the time series, which indicate instances of surface
 156 disturbance or recovery.

157 (3) Age estimation. By pinpointing breakpoints, the time of occurrence for each breakpoint is established. Forest age estimates
 158 for the current location are accomplished by subtracting the breakpoint time from the latest time.

159 LandTrendr was implemented on the GEE platform by using the function of *runLT()* provided by the LT_GEE API (Kennedy
 160 et al., 2018). Table 1 lists the main input parameters.

161 **Table 1.** Parameters of LandTrendr used in this study.

Parameters	Definition	Value
maxSegments	Maximum number of segments to be fitted on the time series	10
spikeThreshold	Threshold for dampening the spikes (1.0 means no dampening)	0.9
vertexCountOvershoot	The initial model can overshoot the maxSegments + 1 vertices by this amount. Later, it will be pruned down to maxSegments + 1	3
preventOneYearRecovery	Prevent segments that represent one-year recoveries	False
recoveryThreshold	If a segment has a recovery rate faster than 1/recovery threshold (in years), then the segment is disallowed	0.25
pvalThreshold	If the p -value of the fitted model exceeds this threshold, then the current model is discarded and another one is fit by using the Levenberg–Marquardt optimizer	0.05
bestModelProportion	Takes the model with most vertices that has a p -value that is at most this fraction away from the model with the lowest p -value	0.75
minObservationsNeeded	Minimum observations required to perform output fitting	6

162

163 2.2.2 Machine learning approach

164 (1) MLA selection

165 This study used the following model-screening procedure to explore which model works best for each vegetation division.
 166 First, we used the automated machine learning (Auto-ML) open-source Python library LazyPredict to filter for alternative
 167 models. LazyRegressor (including 40 MLAs) was used to build stand-age estimation models based on all data, which helps to
 168 understand which MLA works well without tuning parameters. The performing models with R^2 greater than 0.60 in each
 169 vegetation division were concentrated in thirteen MLAs (Supplementary Table 2). Second, by splitting training data and testing
 170 data, the top three MLAs for each vegetation division were determined (Supplementary Table 2). It can be found that the
 171 potential optimal models of eight vegetation divisions is concentrated in RF, Gradient Boosting Decision Tree (GBDT),
 172 Histogram Gradient Boosting (HistGradientBoost), Light Gradient Boosting Machine (LightGBM), and Categorical Boosting
 173 (CatBoost).

174 RF is an ensemble learning method that combines multiple decision trees (Breiman 2001; Dutta et al., 2020). It leverages the
175 wisdom of crowds to make accurate predictions. RF mitigates overfitting and provides robust results by training each tree on
176 a random subset of the data and features (Lavanya et al., 2017; Guo et al., 2019). GBDT is an ensemble technique that builds
177 a strong predictive model by sequentially training decision trees (Jerome 2001). Each tree corrects the errors of its predecessor
178 (Wei et al., 2019), resulting in a highly accurate and robust model. HistGradientBoost is a variant of GBDT that employs
179 histogram-based techniques. It efficiently approximates data distributions and reduces memory consumption during training.
180 This algorithm is particularly beneficial when dealing with large datasets and complex features (Tesfagerish et al., 2022).
181 LightGBM is a gradient-boosting framework that prioritizes speed and efficiency. It employs a histogram-based approach and
182 parallel computing, making it suitable for large datasets. CatBoost is a new modification gradient boosting algorithm that is
183 designed specifically for handling categorical features. It automatically encodes categorical variables, simplifying the data pre-
184 processing stage. CatBoost is known for its robustness and efficiency, can achieve high accuracy on a small-scale dataset.
185 We implemented RF, GBDT, and HistGradientBoost by using the Scikit-learn package of Python 3.9.11, while the LightGBM
186 and CatBoost algorithms were constructed by using the lightgbm and catboost packages of Python 3.9.11.

187 **(2) Hyperparameter tuning**

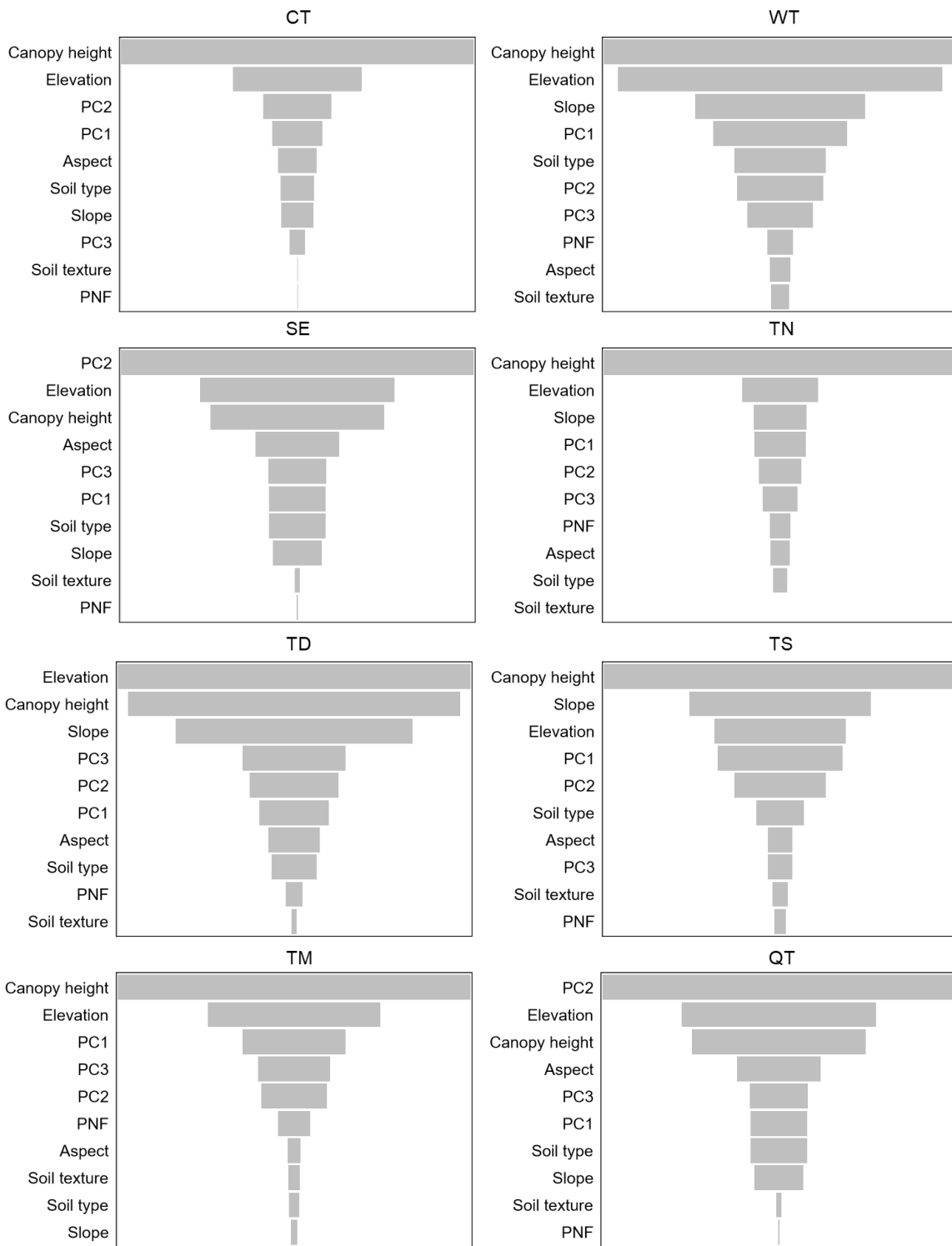
188 Hyperparameter tuning of MLAs is critical in the ML model training process because it significantly enhances the model's
189 performance, generalization capability, and adaptability (Sandha et al., 2020). Bayesian optimization has been selected for
190 hyperparameter tuning due to its complicated derivative evaluation, and nonconvex-function-related features (Mekruksavanich
191 et al., 2022). It is implemented by using Optuna, an open source hyperparameter optimization framework to automate
192 hyperparameter searches (Akiba et al., 2019). The hyperparameters and their searching range in MLAs are listed in
193 Supplementary Table 2.

194 **(3) Model interpretation**

195 Furthermore, we used Shapley Additive explanations (SHAP) values (Lundberg and Lee, 2017; Lundberg et al., 2019), a
196 model-agnostic technique for interpreting ML models, to explore functional correlations between the variables and forest age
197 (Besnard et al. 2021). SHAP derives the Shapely additive contribution values from coalitional game theory (Kim et al. 2023).
198 By examining the contribution of each input variable to the model's output, SHAP can identify the primary drivers of the
199 model's predictions and provide insights into the underlying causes that influence forest age (Sun et al. 2023). The higher the
200 SHAP value, the larger the contribution of the variable. Here we calculated SHAP value using *shap* package in Python.

201 **2.3 Accuracy assessment**

202 **Three independent datasets were used to validate the generated forest age map. The first was collected through forest inventory**
203 **between 2004 and 2008. The second was obtained from the literatures. To ensure the samples collected were representative,**
204 **we excluded samples dated before 2010. The third is the existing forest age map.** As validation metrics, we used the coefficient
205 of determination (R^2), the root mean square error (RMSE), the mean absolute error (MAE), and the mean error (ME). These
206 are given mathematically as

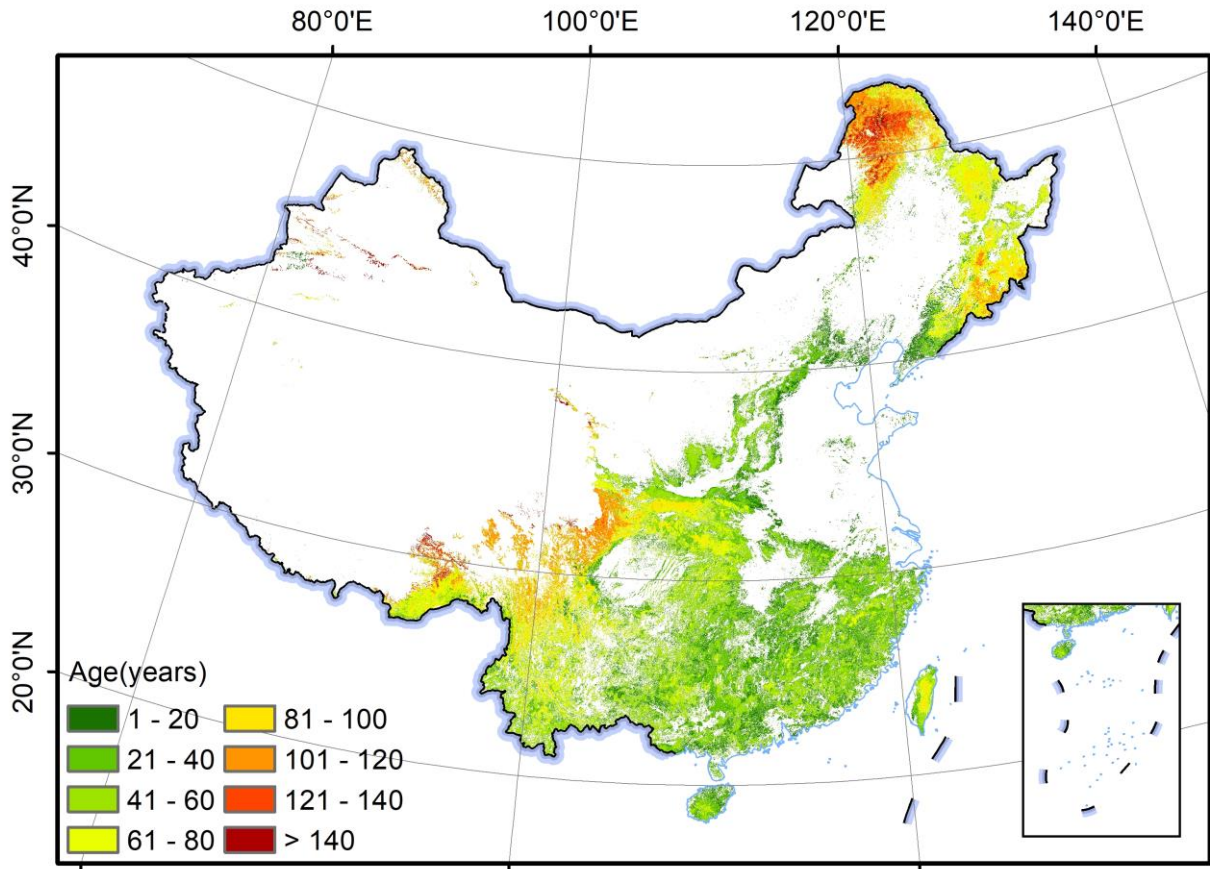


233

234 **Figure 3.** Order of shape values of factors affecting the estimation of forest age in different vegetation zones

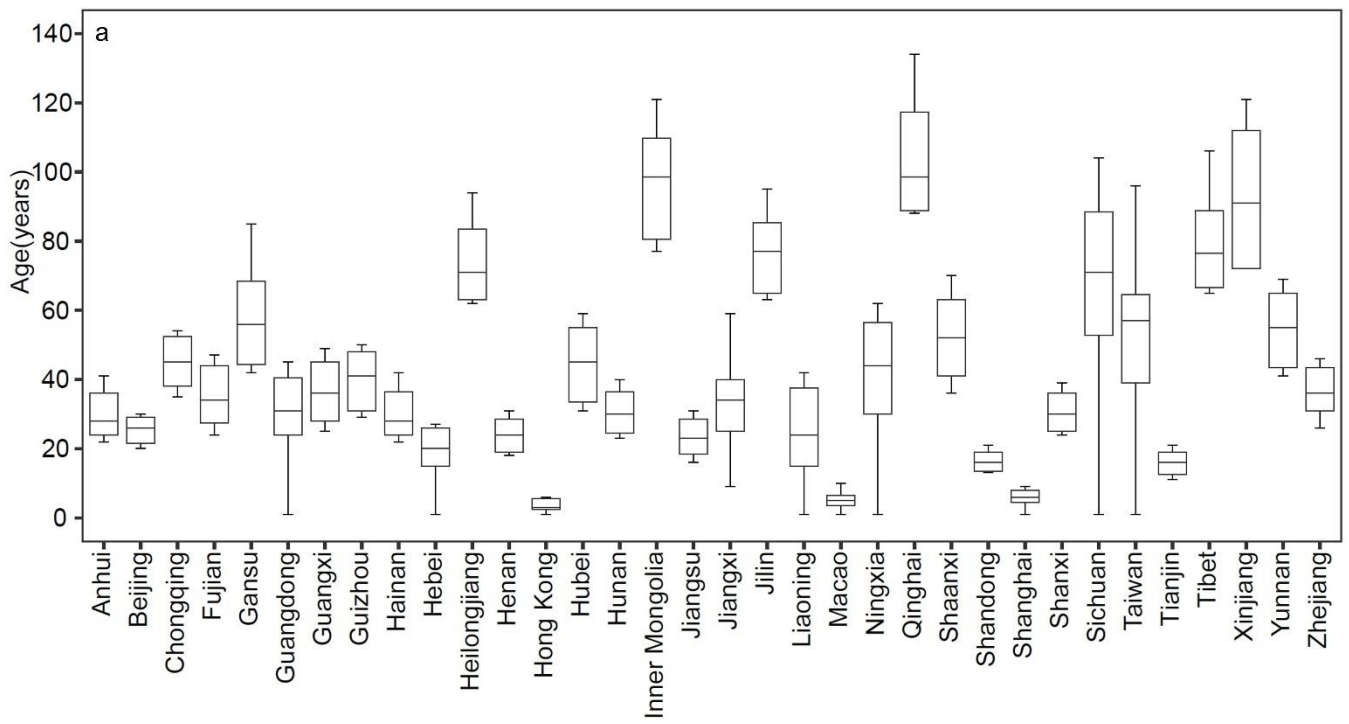
235 **3.2 China's forest age map**

236 China's 30 m resolution forest-age map is presented in [Figure 4](#). The mean of the estimated forest age is 56.11 years with a
237 standard deviation of 32.67 years. Geographically, forests in northeast and southwest China are relatively older than those in
238 other regions ([Figure 4](#)). At the provincial scale, the average forest age ranges from 3.9 to 116.8 years ([Figure 5a](#),
239 [Supplementary Table 5](#)), whereas Qinghai province has the highest mean forest age, and Hong Kong has the lowest mean
240 forest age. Forest ages in Sichuan province are more varied than in other provinces ([Figure 5a](#)). On the regional scale, the QT
241 vegetation zones have the oldest forests with an average of 138.0 years, followed by CT (107.6 years), TS (107.0 years), TN
242 (68.3 years), TD (60.3 years), TM (53.0 years), and SE (49.2 years) ([Figure 5b, Supplementary Table 6](#)). The WT vegetation
243 zones have the youngest forests (28.5 years).

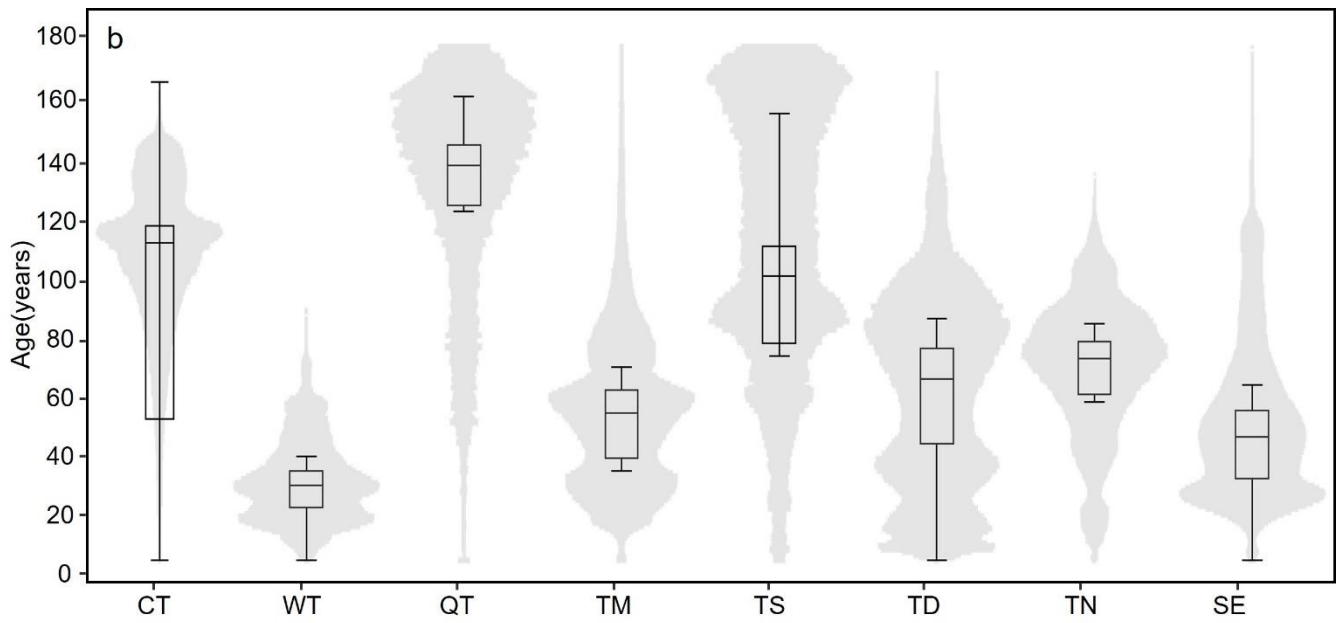


244

245 **Figure 4.** Distribution of China's forest age with 30 m resolution.



246



247

248

Figure 5. (a) Boxplot of China's forest age grouped by provinces (b) Violin plot of the forest age grouped by vegetation divisions.

249 3.3 Evaluation

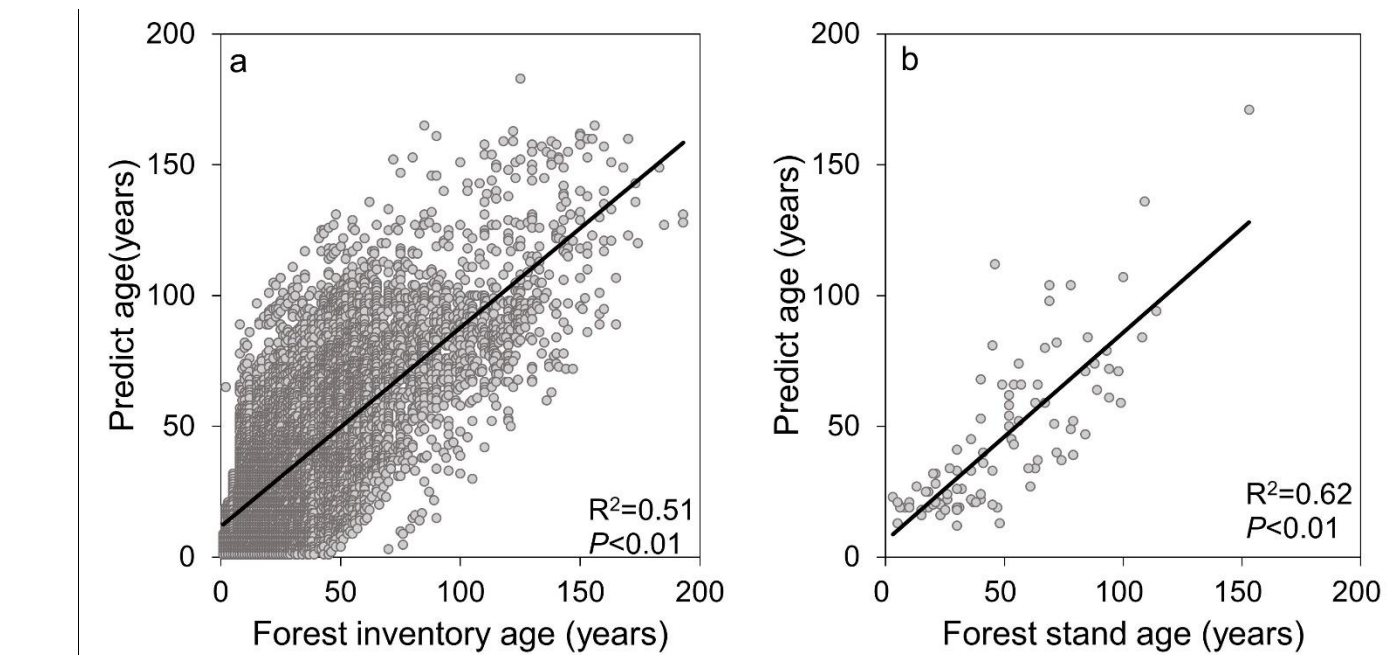
250 We used three independent data sources to evaluate the final forest age map, including forest inventory samples from 2004 to
251 2008, field measurements collected from published papers, and existing forest age products.

252 3.3.1 Comparison with forest inventory samples

253 We initially validated the forest age estimations by using forest inventory data. The forest inventory samples were acquired
254 from 2003 to 2008. To align with the time frame of the forest age data obtained in this study, we shifted the predicted values
255 corresponding to each sample forward by ~16 years. This strategy allows us to compare them with the inventory-measured
256 forest ages. Figure 6a shows the comparison, which suggests that they have a significant linear relationship with $R^2 = 0.51$
257 (Figure 6a).

258 3.3.2 Comparison with field measurements

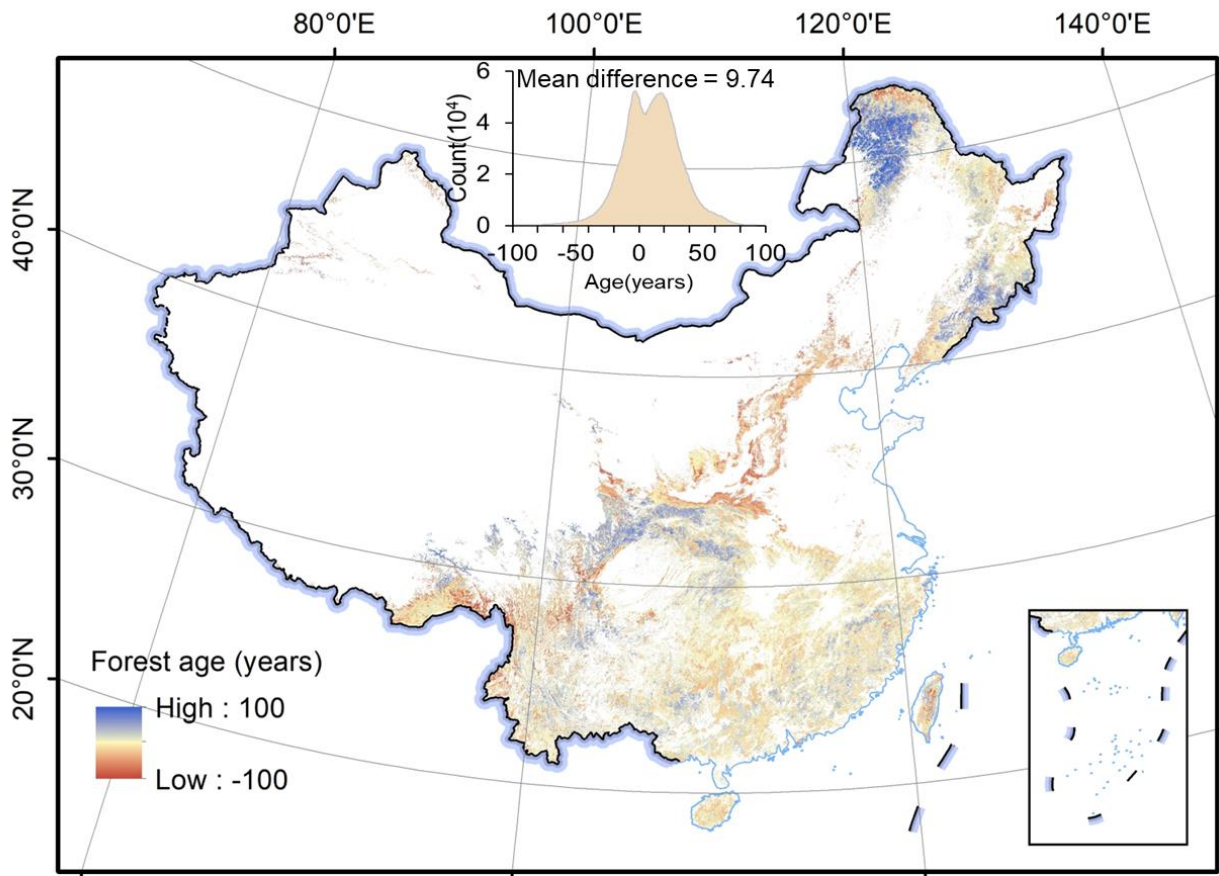
259 We collected 99 field measurements of mean forest stand age after 2010 from published papers (Supplementary Table 7) and
260 compared them with our estimated results. Figure 6b shows that the predicted forest ages also present a significant linear
261 relationship with field measurements, with $R^2 = 0.62$.



262
263 **Figure 6.** Scatter plots of (a) forest inventory age vs predicted forest age for this study and (b) field measurements of forest stand age
264 collected from published papers vs predicted forest.

265 3.3.3 Comparison with existing forest age products

266 We compared our estimated forest age map with an independent global forest age data product produced by Besnard et al.
267 (2021a). Figure 7 shows the difference between these two maps, which suggests an average difference of 9.7 years. Our mapped
268 forest age is older in northeast regions but younger forests in the middle regions than that from Besnard et al. (2021a) dataset.
269 In addition, we gathered the existing forest age maps over China from published datasets and compared their average forest
270 forest age with our estimation (Table 3). According to the available data, the average forest age in China ranged from 40 to 43 years
271 between 2000 and 2013, corresponding to approximately 50 to 53 years in 2020. This aligns closely with the average forest
272 age of 56.1 years obtained in this study for the year of 2020, further underscoring the reliability of the forest age mapped in
273 this study.



274
275 **Figure 7.** Comparison with global forest age product. The inset at the top left shows the frequency distribution of differences between the
276 global forest age map and our estimated forest age map.

277

278 **Table 3.** China's mean forest age collected from published papers.

Source	Mean forest age (years)	Resolution	Mapping year
Zhang et al. (2017)	42.6	1 km	2013
Zhang et al. (2014)	43	1 km	2005
Dai Ming (2011)	40.6	8 km	1998
Wang et al. (2007)	<40	1 km	2001
Xia et al. (2023)	44.0	1 km	2015
This study	56.1	30 m	2020

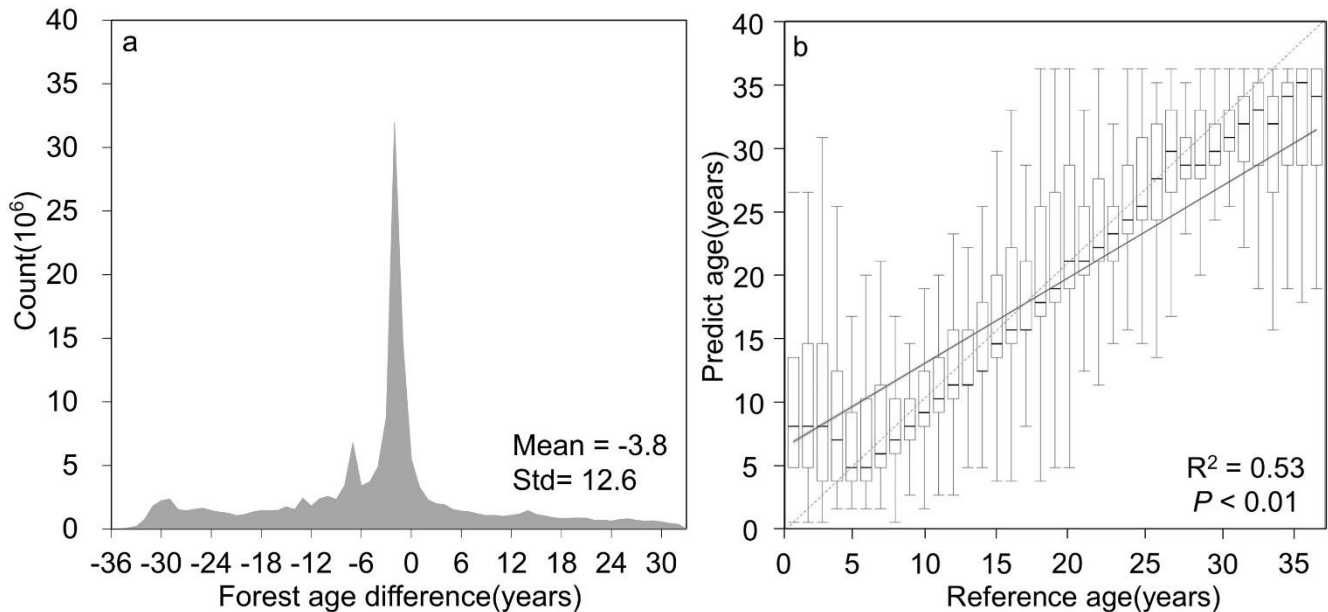
279 **4 Discussion**

280 A high-spatial resolution forest age map is an important input for accurately quantifying forest carbon storage and potential.
 281 Although several forest age maps for China were generated in the most recent decades, their spatial resolution is coarser,
 282 ranging from 1 to 8 km (e.g., Zhang et al., 2014; Zhang et al., 2017), which does not satisfy the application requirements for
 283 local-to-regional scales (Xiao et al., 2023). Therefore, we generated a 30 m resolution forest age map of China using remote
 284 sensing and inventory data for 2020. Validation against independent forest inventory samples, field measurements collected
 285 from published papers, and existing forest age products indicate that the estimated forest age map has R^2 of 0.51 to 0.62, and
 286 presented well spatial agreement with the existing forest age product. Such a high-resolution and timely forest age dataset is
 287 vital to assess ecological benefits of China's forests and to manage forest resources for sustainable development.

288 The generated forest age map indicates that 40.08% of forests are younger than 40 years, 38.11% are 41–80 years old, and
 289 21.81% are over 80 years old. This result indicates that most forests in China are young, which is consistent with the findings
 290 of Zhang et al. (2017) and Zhang et al. (2014), even though the specific proportions might vary slightly, which is mainly
 291 because they produced forest age distribution data for the year of 2005, whereas our data represents forest age in 2020.
 292 Furthermore, similar to Zhang et al. (2017) and Zhang et al. (2014), forests younger than 40 years are primarily in southern
 293 and eastern China, whereas forests older than 80 years are predominantly in northeastern and southwestern China (Figure 4).
 294 We further analyse the forest age by using China's planted and natural forest mask generated by Cheng et al. (2023) for 2020.
 295 The results reveal that the average forest age for planted forests in China is 29.1 years with a standard deviation of 18.2 years,
 296 whereas natural forests have an average age of 69.7 years with a standard deviation of 30.6 years. This result aligns closely
 297 with the reported 16.5 years for China's planted forests in 2005 (which equates to approximately 31 years in 2020) by Yu et
 298 al. (2020b).

299
 300 This study combines two methods to estimate forest age across China. The first method uses time-series remote sensing
 301 imagery and the LandTrendr algorithm to detect pixels that changed within the forest extent from 1985 to 2020. The forest age
 302 was estimated according the time since the last disturbance serving as a proxy for forest age. This approach has been

303 extensively used to estimate forest age and is generally acknowledged to be accurate and reliable for detecting disturbance
304 (Hermosilla et al., 2016). For instance, Du et al. (2022) used the LandTrendr algorithm to detect planting times of global
305 planted forests, and Xiao et al. (2023) estimated the forest age of young forests in China since 1984 by using the CCDC time-
306 series algorithm. These successful cases validate the feasibility of using time-series change-detection algorithms to estimate
307 the age of disturbed forests. In this study, we compared our change-detection derived forest age with the age of young forests
308 provided by Xiao et al. (2023) (Figure 8). These two outcomes have a mean difference of -3.79 years (Figure 8a) and have a
309 significant linear relationship with $R^2 = 0.53$ (Figure 8b). However, this approach only detects the forest age of disturbed areas
310 based on Landsat images; for undisturbed forests, we propose using nonparametric MLAs to estimate forest age. Additionally,
311 considering China's abundant forest resources, wide distribution, and complex terrain, this study proposes an approach to
312 study forest-age estimation models based on MLAs.
313



314
315 **Figure 8.** (a) Age difference and (b) linear relationship between estimated forest age and China's Young Forest Age dataset generated by
316 Xiao et al. (2023).

317 We investigate in-depth the suitability of current mainstream MLAs for estimating forest age. For each vegetation division,
318 we establish the optimal MLA and its optimal parameters (Table 2, Supplementary Table 3). Of the established MLAs, the
319 ensemble learning approaches perform best for both training and evaluation compared with individual-based learners. Several
320 previous studies support the idea that ensemble techniques have achieved better performance than that of its base learners (e.
321 g. Rodriguez et al., 2006; Banfield et al., 2007; Canul-Reich et al., 2007; Rokach, 2009; De Stefano et al., 2011; Matloob et
322 al., 2021). Bagging and boosting are two mainstream ensemble techniques in ensemble learning that combine multiple base
323 models to improve predictive performance. Bagging reduces variance, whereas boosting reduces bias and improves overall
324 model performance (Abbasi et al., 2022). However, most previous studies focus on bagging-based RF models to derive forest

325 structure parameters in remote sensing fields (Simard et al., 2011; Cartus et al., 2012; Montesano et al., 2013; Matasci et al.,
326 2018; Luther et al., 2019; Bolton et al., 2020). The present study highlights that super ensemble learning algorithms based on
327 boosting, including GBDT, LightGBM, and CatBoost, demonstrate higher accuracy in estimating China's forest age compared
328 to the bagging-based RF algorithm. Furthermore, within the current ensemble learning framework, the CatBoost algorithm
329 based on boosting has a clear advantage for estimating forest age in China (Table 2). It produces optimal results in five
330 vegetation zones and is as accurate as the best-performing algorithms in the remaining vegetation zones (Supplementary Table
331 4). Therefore, we recommend giving priority to the utilization of the CatBoost algorithm in deriving the forest structural
332 parameters in China.

333

334 In the process of machine learning modelling for forest age estimation, we selected a total of 10 features, including canopy
335 height, meteorological factors, soil factors, terrain factors, and human activities. Factor analysis indicates that canopy height
336 has significantly influence forest age modelling, which is consistent with previous research, such as Zhang et al. (2017), who
337 estimated forest age in China based on the relationship between canopy height and forest age. The main reason is that canopy
338 height is typically correlated with the growth period (Sharma and Parton, 2007; Schumacher et al., 2020b; Lin et al., 2023).
339 Young trees usually have shorter canopy height and, as trees age, canopy height gradually increases (Yu et al., 2020b).
340 Therefore, canopy height gives clues about tree age, and many age-estimation models are based on forest height (Lin et al.,
341 2023). Terrain conditions also play important roles in all vegetation zones, especially the elevation and slope features (Figure
342 2). This is mainly because terrain factors are closely related to vegetation distribution, growth conditions, and hydrological
343 processes (Fernández-Martínez et al., 2014) and affecting forest age estimation (Lin et al., 2008). Climate factors, including
344 temperature and precipitation, also play a significant role in estimating forest age and have been applied to estimate global
345 forest age (Besnard et al., 2021a). Climate elements are most pronounced in the SE and QT vegetation zones because these
346 two zones belong to areas with extreme climates and pronounced seasonal variations (Zhang et al., 2018). The SE region has
347 a warm and humid climate with abundant rainfall (Zhang et al., 2018), which aligns with seasonal growth, making it influential
348 in forest age estimation. The QT region experiences extreme temperature fluctuations, with extremely cold winters and short
349 and cool summers, significantly affecting tree growth rates and cycles (Zhang et al., 2021). Although soil and human activities
350 seem to have a relatively smaller impact in this study, the high accuracy achieved in this study is attributed to the combined
351 contributions of all factors.

352

353 Overall, we produce a reliable forest age map for China. This forest age product has been validated by independent field
354 samples and compared against existing datasets with a R^2 ranging from 0.51 to 0.62 (Figure 6). However, it is imperative to
355 acknowledge that intrinsic uncertainties arise from data-related constraints. Primarily, the utilization of forest mask that
356 delineate planted and natural forests introduces an inescapable source of uncertainty, which is particularly high (approximately
357 10%) in the southern regions of China (Cheng et al., 2023a). Furthermore, the dependence on canopy-height data generated
358 by Liu et al. (2022) as the crucial determinant in forest age estimation (Figure 2) necessitates meticulous consideration (Zhang

359 et al., 2017), giving the uncertainties in the canopy-height data ($R^2=0.55$) could strongly affect the accuracy in forest age
360 modelling. Finally, when benchmarked against extant products, conspicuous disparities in forest age estimates appear within
361 the northeastern and southwestern regions (Figure 6). These disparities, coupled with insights from forest inventory data,
362 highlight the prevalence of older forests (exceeding 100 years) within these regions (Figures 1 and 4). The unique challenge
363 posed by estimating the age of such older forests, characterized by sluggish growth rates (Maltman et al., 2023b), accentuates
364 the sensitivity to crown height data. Consequently, the uncertainty associated with canopy height data is conspicuously
365 accentuated in these regions.

366 **5 Data availability**

367 The 30 m resolution forest age map of China generated by this study is openly available at
368 <https://doi.org/10.5281/zenodo.8354262> (Cheng et al., 2023b). Please contact the authors for more detailed information

369 **6 Conclusion**

370 High-resolution and spatially explicit forest age mapping for China play a crucial role in accurately quantifying the current
371 carbon sequestration of forest ecosystems and its potential in the future. Currently, publicly available China's forest age data
372 suffer from low resolution and incomplete coverage of age ranges, making it difficult to meet the requirements of studies at
373 various spatial scales. Therefore, this study combines time-series analysis of remote sensing imagery with MLAs to create the
374 first 30 m resolution China's forest age map for the year of 2020. Validation against forest inventory data, field measurements,
375 and existing products demonstrates the R^2 values between 0.51 and 0.62. The estimated forest age data reveal an average forest
376 age of 56.1 years for China, with a standard deviation of 32.7 years. This dataset holds significant importance for understanding
377 the carbon source and sink dynamics in China's forest ecosystem.

378

379 **Author contributions**

380 KC, YC and QG designed the research. KC, YC, TX performed the analysis, KC and YC wrote the paper. QG, HY, and QM
381 supervised and reviewed the paper. HG and YR reviewed the manuscript. QG, KC, YC, WL collected the field measurements
382 and existing remote sensing products. KC and YC contributed equally to this work.

383 **Competing interests**

384 The contact author has declared that none of the authors has any competing interests.

385 **Acknowledgements**

386 We would like to thank the editor and the two reviewers for their valuable comments.

387

388 **Financial support**

389 This research has been supported by the National Key Research and Development Program of China (grant no.
390 2022YFF130203), the International Research Center of Big Data for Sustainable Development Goals (grant no.
391 CBAS2022GSP06), the National Natural Science Foundation of China (grant no. 42371329 and 31971575).

392 **References**

- 393 Abbasi, E., M. R. Alavi Moghaddam, and E. Kowsari. A systematic and critical review on development of machine learning
394 based-ensemble models for prediction of adsorption process efficiency. *J. Clean. Prod.*, 379:134588,
395 <https://doi.org/10.1016/j.jclepro.2022.134588>, 2022
- 396 Akiba, T., S. Sano, T. Yanase, T. Ohta, and M. Koyama. Optuna: A Next-generation Hyperparameter Optimization Framework.
397 Pages 2623–2631 Proceedings of the 25th ACM SIGKDD International Conference on Knowledge Discovery & Data
398 Mining. Association for Computing Machinery, Anchorage, AK, USA. <https://doi.org/10.48550/arXiv.1907.10902>, 2019.
- 399 Alerskans, E., A.-S. P. Zinck, P. Nielsen-Englyst, and J. L. Høyer. Exploring machine learning techniques to retrieve sea
400 surface temperatures from passive microwave measurements. *Remote Sens Environ.*, 281:113220,
401 <https://doi.org/10.1016/j.rse.2022.113220>, 2022.
- 402 Banfield, R. E., L. O. Hall, K. W. Bowyer, and W. P. Kegelmeyer. A Comparison of Decision Tree Ensemble Creation
403 Techniques. *IEEE Trans. Pattern Anal. Mach. Intell.*, 29:173-180, <https://doi.org/10.1109/TPAMI.2007.250609>, 2007.
- 404 Besnard, S., S. Koirala, M. Santoro, U. Weber, J. Nelson, J. Gutter, B. Hérault, J. Kassi, A. N’Guessan, C. Neigh, B. Poulter,
405 T. Zhang, and N. Carvalhais. Mapping global forest age from forest inventories, biomass and climate data. *Earth Syst. Sci.*
406 *Data.*, 13:4881-4896, <https://doi.org/10.5194/essd-13-4881-2021>, 2021a.
- 407 Bolton, D. K., P. Tompalski, N. C. Coops, J. C. White, M. A. Wulder, T. Hermosilla, M. Queinnec, J. E. Luther, O. R. van
408 Lier, R. A. Fournier, M. Woods, P. M. Treitz, K. Y. van Ewijk, G. Graham, and L. Quist. Optimizing Landsat time series
409 length for regional mapping of lidar-derived forest structure. *Remote Sens Environ.*, 239:111645,
410 <https://doi.org/10.1016/j.rse.2020.111645>, 2020.
- 411 Breiman, L. Random Forests. *Machine Learning* 45:5-32, <https://doi.org/10.1023/A:1010933404324>, 2001.
- 412 Canul-Reich, J., L. Shoemaker, and L. O. Hall. Ensembles of Fuzzy Classifiers. Pages 1-6 in 2007 IEEE International Fuzzy
413 Systems Conference. <https://doi.org/10.1109/FUZZY.2007.4295345>, 2007.

414 Cartus, O., J. Kellndorfer, M. Rombach, and W. Walker. Mapping Canopy Height and Growing Stock Volume Using Airborne
415 Lidar, ALOS PALSAR and Landsat ETM+. *Remote Sens.*, 4:3320-3345, <https://doi.org/10.3390/rs4113320>, 2012.

416 Cheng, K., Y. Su, H. Guan, S. Tao, Y. Ren, T. Hu, K. Ma, Y. Tang, and Q. Guo. Mapping China's planted forests using high
417 resolution imagery and massive amounts of crowdsourced samples. *ISPRS J. Photogramm. Remote Sens.*, 196:356-371,
418 <https://doi.org/10.1016/j.isprsjprs.2023.01.005>, 2023a.

419 Cheng, K, Y, Chen, T, Xiang, H, Yang, W, Liu, Y, Ren, H, Guan, T, Hu, Q, Ma, and Qinghua Guo. 2020 forest age map for
420 China with 30 m resolution (1.0) [Data set]. Zenodo. <https://doi.org/10.5281/zenodo.8354262>, 2023b.

421 Dai, M., T. Zhou, L. Yang, and G. Jia. Spatial pattern of forest ages in China retrieved from national-level inventory and
422 remote sensing imageries. *GEOGRAPHICAL RESEARCH* 30:172-184, <https://doi.org/10.11821/yj2011010017>, 2011 (in
423 Chinese).

424 De Stefano, C., F. Fontanella, G. Folino, and A. S. di Freca. A Bayesian Approach for Combining Ensembles of GP Classifiers.
425 Pages 26-35. Springer Berlin Heidelberg, Berlin, Heidelberg. https://doi.org/10.1007/978-3-642-21557-5_5, 2011.

426 Du, Z., L. Yu, J. Yang, D. Coomes, K. Kanniah, H. Fu, and P. Gong. Mapping Annual Global Forest Gain From 1983 to 2021
427 With Landsat Imagery. *IEEE J-STARS.*, 16:4195-4204, <https://doi.org/10.1109/JSTARS.2023.3267796>, 2023.

428 Du, Z., L. Yu, J. Yang, Y. Xu, B. Chen, S. Peng, T. Zhang, H. Fu, N. Harris, and P. Gong. A global map of planting years of
429 plantations. *Scientific Data.*, 9:141, <https://doi.org/10.1038/s41597-022-01260-2>, 2022.

430 Dutta, K. K., S. S. A, A. Victor, A. G. Nathu, M. A. Habib, and D. Parashar. Kannada Alphabets Recognition using Decision
431 Tree and Random Forest Models. Pages 534-541 in 2020 3rd International Conference on Intelligent Sustainable Systems
432 (ICISS). <https://doi.org/10.1109/ICISS49785.2020.9315972>, 2020.

433 Fernández-Martínez, M., S. Vicca, I. A. Janssens, S. Luysaert, M. Campioli, J. Sardans, M. Estiarte, and J. Peñuelas. Spatial
434 variability and controls over biomass stocks, carbon fluxes, and resource-use efficiencies across forest ecosystems. *Trees.*
435 28:597-611, <https://doi.org/10.1007/s00468-013-0975-9>, 2014.

436 Guo, Y., Y. Zhou, X. Hu, and W. Cheng. Research on Recommendation of Insurance Products Based on Random Forest.
437 Pages 308-311 in 2019 International Conference on Machine Learning, Big Data and Business Intelligence (MLBDBI).
438 <https://doi.org/10.1109/MLBDBI48998.2019.00069>, 2019.

439 Hermosilla, T., M. A. Wulder, J. C. White, N. C. Coops, G. W. Hobart, and L. B. Campbell. Mass data processing of time
440 series Landsat imagery: pixels to data products for forest monitoring. *Int J Digit Earth.*, 9:1035-1054,
441 <https://doi.org/10.1080/17538947.2016.1187673>, 2016.

442 Jerome, H. F. Greedy function approximation: A gradient boosting machine. *Ann Stat.*, 29:1189-1232,
443 <https://doi.org/10.1214/aos/1013203451>, 2001.

444 Kennedy, R. E., Z. Yang, N. Gorelick, J. Braaten, L. Cavalcante, W. B. Cohen, and S. Healey. Implementation of the
445 LandTrendr Algorithm on Google Earth Engine. *Remote Sens.*, 10:691, <https://doi.org/10.3390/rs10050691>, 2018.

446 Kim, Hyunglok, Wade Crow, Xiaojun Li, Wolfgang Wagner, Sebastian Hahn, and Venkataraman Lakshmi. True global error
447 maps for SMAP, SMOS, and ASCAT soil moisture data based on machine learning and triple collocation analysis. *Remote*
448 *Sens Environ.*, 298: 113776, <https://doi.org/10.1016/j.rse.2023.113776>, 2023.

449 Lavanya, K., S. Bajaj, P. Tank, and S. Jain. Handwritten digit recognition using hoeffding tree, decision tree and random
450 forests — A comparative approach. Pages 1-6 in 2017 International Conference on Computational Intelligence in Data
451 Science (ICCIDS). <https://doi.org/10.1109/ICCIDS.2017.8272641>, 2017.

452 Lin, G., B. Xia, Z. Zeng, and W. Huang. The Relationship between NDVI, Stand Age and Terrain Factors of *Pinus elliottii*
453 Forest. Pages 232-236 in 2008 International Workshop on Education Technology and Training & 2008 International
454 Workshop on Geoscience and Remote Sensing. <https://doi.org/10.1109/ETTandGRS.2008.302>, 2008.

455 Lin, X., R. Shang, J. M. Chen, G. Zhao, X. Zhang, Y. Huang, G. Yu, N. He, L. Xu, and W. Jiao. High-resolution forest age
456 mapping based on forest height maps derived from GEDI and ICESat-2 space-borne lidar data. *Agric For Meteorol.*,
457 339:109592, <https://doi.org/10.1016/j.agrformet.2023.109592>, 2023.

458 Liu, X., Y. Su, T. Hu, Q. Yang, B. Liu, Y. Deng, H. Tang, Z. Tang, J. Fang, and Q. Guo. Neural network guided interpolation
459 for mapping canopy height of China's forests by integrating GEDI and ICESat-2 data. *Remote Sens Environ.*, 269,
460 <https://doi.org/10.1016/j.rse.2021.112844>, 2022.

461 Lundberg, S. and Lee, S.-I. A Unified Approach to Interpreting Model Predictions, arXiv [preprint], arXiv:1705.07874,
462 <https://doi.org/10.48550/arXiv.1705.07874>, 2017.

463 Lundberg, S. M., Erion, G. G., and Lee, S.-I. Consistent Individualized Feature Attribution for Tree Ensembles, arXiv
464 [preprint], arXiv:1802.03888, <https://doi.org/10.48550/arXiv.1802.03888>, 2019

465 Luther, J. E., R. A. Fournier, O. R. van Lier, and M. Bujold. Extending ALS-Based Mapping of Forest Attributes with Medium
466 Resolution Satellite and Environmental Data. *Remote Sens.*, 11:1092, <https://doi.org/10.3390/rs11091092>, 2019.

467 Maltamo, M., H. Kinnunen, A. Kangas, and L. Korhonen. Predicting stand age in managed forests using National Forest
468 Inventory field data and airborne laser scanning. *For. Ecosyst.*, 7:44, <https://doi.org/10.1186/s40663-020-00254-z>, 2020.

469 Maltman, J. C., T. Hermosilla, M. A. Wulder, N. C. Coops, and J. C. White. Estimating and mapping forest age across Canada's
470 forested ecosystems. *Remote Sens Environ.*, 290:113529, <https://doi.org/10.1016/j.rse.2023.113529>, 2023a.

471 Matasci, G., T. Hermosilla, M. A. Wulder, J. C. White, N. C. Coops, G. W. Hobart, and H. S. J. Zald. Large-area mapping of
472 Canadian boreal forest cover, height, biomass and other structural attributes using Landsat composites and lidar plots.
473 *Remote Sens Environ.*, 209:90-106, <https://doi.org/10.1016/j.rse.2017.12.020>, 2018.

474 Matloob, F., T. M. Ghazal, N. Taleb, S. Aftab, M. Ahmad, M. A. Khan, S. Abbas, and T. R. Soomro. Software Defect
475 Prediction Using Ensemble Learning: A Systematic Literature Review. *IEEE Access*, 9:98754-98771,
476 <https://doi.org/10.1109/ACCESS.2021.3095559>, 2021.

477 Mekruksavanich, S., P. Jantawong, N. Hnoohom, and A. Jitpattanakul. Hyperparameter Tuning in Convolutional Neural
478 Network for Face Touching Activity Recognition using Accelerometer Data. Pages 101-105 in 2022 Research, Invention,

479 and Innovation Congress: Innovative Electricals and Electronics (RI2C). <https://doi.org/10.1109/RI2C56397.2022.9910262>,
480 2022.

481 Montesano, P. M., B. D. Cook, G. Sun, M. Simard, R. F. Nelson, K. J. Ranson, Z. Zhang, and S. Luthcke. Achieving accuracy
482 requirements for forest biomass mapping: A spaceborne data fusion method for estimating forest biomass and LiDAR
483 sampling error. *Remote Sens Environ.*, 130:153-170, <https://doi.org/10.1016/j.rse.2012.11.016>, 2013.

484 Niu, Y., V. Squires, and A. Jentsch. Risks of China's increased forest area. *Science*, 379:447-448,
485 <https://doi.org/10.1126/science.adg0210>, 2023.

486 Pan, Y., R. A. Birdsey, J. Fang, R. Houghton, P. E. Kauppi, W. A. Kurz, O. L. Phillips, A. Shvidenko, S. L. Lewis, J. G.
487 Canadell, P. Ciais, R. B. Jackson, S. W. Pacala, A. D. McGuire, S. Piao, A. Rautiainen, S. Sitch, and D. Hayes. A Large and
488 Persistent Carbon Sink in the World. *Forests. Science*, 333:988-993, <https://doi.org/10.1126/science.1201609>, 2011.

489 Piao, S., Y. He, X. Wang, and F. Chen. Estimation of China's terrestrial ecosystem carbon sink: Methods, progress and
490 prospects. *Sci. China Earth Sci.*, 65:641 – 651, <https://doi.org/10.1007/s11430-021-9892-6>, 2022.

491 Ren, Y., Wei, X., Zhang, L., Cui, S., Chen, F., Xiong, Y., & Xie, P. Potential for forest vegetation carbon storage in Fujian
492 Province, China, determined from forest inventories. *Plant Soil.*, 345, 125-140, <https://doi.org/10.1007/s11104-011-0766-2>,
493 2011.

494 Rodriguez, J. J., L. I. Kuncheva, and C. J. Alonso. Rotation Forest: A New Classifier Ensemble Method. *IEEE Trans. Pattern*
495 *Anal. Mach. Intell.*, 28:1619-1630, <https://doi.org/10.1109/TPAMI.2006.211>, 2006.

496 Rokach, L. Taxonomy for characterizing ensemble methods in classification tasks: A review and annotated bibliography.
497 *Computational Statistics & Data Analysis*, 53:4046-4072, <https://doi.org/10.1016/j.csda.2009.07.017>, 2009.

498 Sandha, S. S., M. Aggarwal, I. Fedorov, and M. Srivastava. Mango: A Python Library for Parallel Hyperparameter Tuning.
499 Pages 3987-3991 in ICASSP 2020 - 2020 IEEE International Conference on Acoustics, Speech and Signal Processing
500 (ICASSP), <https://doi.org/10.1109/ICASSP40776.2020.9054609>, 2020.

501 Schumacher, J., M. Hauglin, R. Astrup, and J. Breidenbach. Mapping forest age using National Forest Inventory, airborne
502 laser scanning, and Sentinel-2 data. *For. Ecosyst.*, 7:60, <https://doi.org/10.1186/s40663-020-00274-9>, 2020a.

503 Sharma, M., and J. Parton. Height–diameter equations for boreal tree species in Ontario using a mixed-effects modelling
504 approach. *For. Ecol. Manag.*, 249:187-198, <https://doi.org/10.1016/j.foreco.2007.05.006>, 2007.

505 Simard, M., N. Pinto, J. B. Fisher, and A. Baccini. Mapping forest canopy height globally with spaceborne lidar. *J. Geophys.*
506 *Res. Biogeosci.*, 116, <https://doi.org/10.1029/2011JG001708>, 2011.

507 Su, Y., Q. Guo, T. Hu, H. Guan, S. Jin, S. An, X. Chen, K. Guo, Z. Hao, Y. Hu, Y. Huang, M. Jiang, J. Li, Z. Li, X. Li, X. Li,
508 C. Liang, R. Liu, Q. Liu, H. Ni, S. Peng, Z. Shen, Z. Tang, X. Tian, X. Wang, R. Wang, Z. Xie, Y. Xie, X. Xu, X. Yang, Y.
509 Yang, L. Yu, M. Yue, F. Zhang, and K. Ma. An updated Vegetation Map of China (1:1000000). *Sci. Bull.*, 65:1125-1136,
510 <https://doi.org/10.1016/j.scib.2020.04.004>, 2020.

511 Sun, Bochao, Wenjun Cui, Gaoyang Liu, Biao Zhou, and Weijian Zhao. A hybrid strategy of AutoML and SHAP for automated
512 and explainable concrete strength prediction. *Case Stud. Constr. Mater.*, 19: e02405,
513 <https://doi.org/10.1016/j.cscm.2023.e02405>, 2023.

514 Tesfagergish, S. G., J. Kapočičūtė-Dzikienė, and R. Damaševičius. Zero-Shot Emotion Detection for Semi-Supervised
515 Sentiment Analysis Using Sentence Transformers and Ensemble Learning. *Appl. Sci.*, 12(17), 8662,
516 <https://doi.org/10.3390/app12178662>, 2022.

517 Tian, L., L. Liao, Y. Tao, X. Wu, and M. Li. Forest Age Mapping Using Landsat Time-Series Stacks Data Based on Forest
518 Disturbance and Empirical Relationships between Age and Height. *Remote Sens.*, 15:2862,
519 <https://doi.org/10.3390/rs15112862>, 2023.

520 Tong, X., M. Brandt, Y. Yue, P. Ciais, M. Rudbeck Jepsen, J. Penuelas, J.-P. Wigneron, X. Xiao, X.-P. Song, S. Horion, K.
521 Rasmussen, S. Saatchi, L. Fan, K. Wang, B. Zhang, Z. Chen, Y. Wang, X. Li, and R. Fensholt. Forest management in
522 southern China generates short term extensive carbon sequestration. *Nat. Commun.*, 11, <https://doi.org/10.1038/s41467-019-13798-8>, 2020.

524 Tubiello, F. N., G. Conchedda, L. Casse, P. Hao, G. De Santis, and Z. Chen. A new cropland area database by country circa
525 2020. *Earth Syst. Sci. Data Discuss.*, 2023:1-33, <https://doi.org/10.5194/essd-2023-211>, 2023.

526 Wang, S., J. M. Chen, W. M. Ju, X. Feng, M. Chen, P. Chen, and G. Yu. Carbon sinks and sources in China's forests during
527 1901–2001. *J. Environ. Manage.*, 85:524-537, <https://doi.org/10.1016/j.jenvman.2006.09.019>, 2007.

528 Wang, Y., X. Wang, K. Wang, F. Chevallier, D. Zhu, J. Lian, Y. He, H. Tian, J. Li, J. Zhu, S. Jeong, and J. G. Canadell. The
529 size of the land carbon sink in China. *Nature*, 603:E7-E9, <https://doi.org/10.1038/s41586-021-04255-y>, 2022.

530 Wei, Z., Y. Meng, W. Zhang, J. Peng, and L. Meng. Downscaling SMAP soil moisture estimation with gradient boosting
531 decision tree regression over the Tibetan Plateau. *Remote Sens Environ.*, 225:30-44,
532 <https://doi.org/10.1016/j.rse.2019.02.022>, 2019.

533 Xia, J., X. Xia, Y. Chen, R. Shen, Z. Zhang, B. Liang, J. Wang, and W. Yuan. Reconstructing Long-Term Forest Age of China
534 by Combining Forest Inventories, Satellite-Based Forest Age and Forest Cover Data Sets. *J. Geophys. Res. Biogeosci.*, 128:
535 e2023JG007492, <https://doi.org/10.1029/2023JG007492>, 2023.

536 Xiao, Y., Q. Wang, X. Tong, and P. M. Atkinson. Thirty-meter map of young forest age in China. *Earth Syst. Sci. Data.*,
537 15:3365-3386, <https://doi.org/10.5194/essd-15-3365-2023>, 2023.

538 Yu, Z., H. R. Zhao, S. R. Liu, G. Y. Zhou, J. Y. Fang, G. R. Yu, X. L. Tang, W. T. Wang, J. H. Yan, G. X. Wang, K. P. Ma,
539 S. G. Li, S. Du, S. J. Han, Y. X. Ma, D. Q. Zhang, J. X. Liu, S. Z. Liu, G. W. Chu, Q. M. Zhang, and Y. L. Li. Mapping
540 forest type and age in China's plantations. *Sci. Total Environ.*, 744. <https://doi.org/10.1016/j.scitotenv.2020.140790>, 2020b.

541 Zhang H, J. Y, , Shen X, Li G, and Z. D. Rising Air Temperature and Its Asymmetry Under Different Vegetation Regions in
542 China. *Sci. Geol. Sin.*, 38 (2): 272-283, <https://doi.org/10.13249/j.cnki.sgs.2018.02.014>, 2018.

543 Zhang, C., W. Ju, J. M. Chen, D. Li, X. Wang, W. Fan, M. Li, and M. Zan. Mapping forest stand age in China using remotely
544 sensed forest height and observation data. *J. Geophys. Res. Biogeosci.*, 119:1163-1179,
545 <https://doi.org/10.1002/2013JG002515>, 2014.

546 Zhang, Y., Y. Yao, X. Wang, Y. Liu, and S. Piao. Mapping spatial distribution of forest age in China. *Earth Space Sci.*, 4:108-
547 116, <https://doi.org/10.1002/2016EA000177>, 2017.

548 Zhang, Z., F. Zhang, L. Wang, A. Lin, and L. Zhao. Biophysical climate impact of forests with different age classes in mid-
549 and high-latitude North America. *For. Ecol. Manag.*, 494:119327. <https://doi.org/10.1016/j.foreco.2021.119327>, 2021.

550